Sensors and Materials, Vol. 30, No. 4 (2018) 939–946
MYU Tokyo

S & M 1552

Resistance Study of Er-doped Zinc Oxide Diode by Spray Pyrolysis

Tzu-Hsiang Lin,[1] Wen-How Lan,[1*] Ming-Chang Shih,[1] Mu-Chun Wang,[2**]
Kuo-Jen Chang,[3] Jia-Ching Lin,[3] Shao-Yi Lee,[3] Wen-Jen Lin,[3] and Chien-Jung Huang[4]

[1]Department of Electrical Engineering, National University of Kaohsiung,
No. 700, Kaohsiung University Road, Nan-tzu District, Kaohsiung 81148, Taiwan (R.O.C.)
[2]Department of Electronic Engineering, Minghsin University of Science and Technology,
No. 1, Xinxing Rd., Xinfeng Township, Hsinchu 30401, Taiwan (R.O.C.)
[3]National Chung-Shan Institute of Science & Technology,
No. 481, Zhongzheng Rd., Longtan District, Taoyuan 32546,Taiwan (R.O.C.)
[4]Department of Applied Physics, National University of Kaohsiung,
No. 700, Kaohsiung University Rd., Nan-tzu District, Kaohsiung 81148, Taiwan (R.O.C.)

(Received November 17, 2017; accepted January 18, 2018)

Keywords: resistance, zinc oxide, erbium

Undoped and erbium-doped zinc oxide followed by indium-doped zinc oxide layers on p-type Si substrate were prepared by spray pyrolysis with zinc acetate, erbium acetate, and indium nitrate precursors. The surface morphology and crystalline quality were investigated. Using a front- and back-side metallization process, diodes were fabricated. The current–voltage characteristics of these diodes were analyzed. The structural resistance, which is an important issue in gas sensing application, shows an increase–decrease behavior with the increase of erbium contents in zinc oxide. With a reverse bias in excess of 6 V, two distinct green light emissions with 536 and 555 nm wavelength and one red light emission at around 664 nm of the 5% erbium-doped zinc oxide diode can be observed. The structural resistance character, as well as the ideality factor of these diodes were analyzed and discussed.

1. Introduction

Zinc oxide (ZnO), a group II–VI semiconductor with high melting temperature,[(1)] wide bandgap,[(2)] and large exciton binding energy,[(3)] has attracted much attention in the past decade. Many ZnO-based devices have been investigated.[(4–9)] In the device structure, the doping in the film is an important issue in the material and device performance. Rare-earth erbium (Er) doping, which improves the resistance response[(10,11)] of ZnO in different gases, has been applied in many gas sensing devices.[(12,13)] Meanwhile, with the carrier transitions between the ionized Er energy states,[(14,15)] photon emissions can be observed.[(16,17)] These Er-related emissions occurred from the energy transformation of electron–hole pairs and/or electron impact to Er ion under suitable voltage bias.[(18,19)]

*Corresponding author: e-mail: whlan@nuk.edu.tw
**Corresponding author: e-mail: mucwang@must.edu.tw
http://dx.doi.org/10.18494/SAM.2018.1809

ISSN 0914-4935 © MYU K.K.

In the fabrication of ZnO thin film, many deposition methods such as molecular beam epitaxy,[20] chemical vapor deposition,[21] sputtering,[22] sol–gel,[23] and spray pyrolysis[24] have been developed. The spray pyrolysis method, which is one of the nonvacuum techniques, shows potential for easy scale up.

In our previous study, we examined the conduction type and concentrations of the Er-doped ZnO thin films. In this work, we report the electrical properties of the p-Si/n-ZnO:Er heterojunction diode with different Er contents by spray pyrolysis. The effects of Er doping, diode resistance, ideality factor, and electroluminescence properties were discussed.

2. Experimental Details

ZnO:Er/ZnO:In diodes with different Er contents were grown on p-Si [(111), 5×10^{18} cm^{-3}] substrates by spray pyrolysis deposition.[24] Aqueous solutions containing zinc acetate [$Zn(CH_3COOH)_2 \cdot 2H_2O$], erbium acetate [$Er(CH_3COO)_3 \cdot 4H_2O$], and indium nitrate [$In(NO_3)_3 \cdot 5H_2O$] were used as precursors in the fabrication of ZnO:Er and ZnO:In layers. The Zn concentration was fixed at 0.2 M in precursors. Before deposition, the aqueous solution was stirred for one hour at room temperature to yield a clear solution. In the ZnO:Er layer, the atomic ratios of Er to Zn in the precursor were 0, 1, 5, and 10%.[25] In the ZnO:In layer, the atomic ratio of In to Zn in the precursor was 5% for all samples. The deposition temperature was 450 °C. The thicknesses of ZnO:Er and ZnO:In are around 400 and 40 nm, respectively. The concentration of ZnO:In was around 5×10^{18} cm^{-3}. After the film deposition, In was deposited on the backside of Si using a thermal coater. The front Au circular pads of 0.8 mm diameter were achieved with a shadow mask on the ZnO:In surface by direct-current magnetron sputtering. The samples with different Er contents were then indexed as S0, S1, S2, and S3.

The surface morphology of the films was examined by scanning electron microscopy (SEM, HITACHI S-4300N). The crystalline property was examined by X-ray diffraction (XRD, Bruker D8). The photoluminescence (PL) measurement was accomplished using an optical system with a spectrometer (Ocean, HR2000+) , a He-Cd laser (325 nm wavelength) as the light source, and a temperature-controlled cryogenic system. The source meter (Keithley 2400) was applied in the device current–voltage measurement.

3. Results and Discussion

Figure 1 shows the XRD pattern of the ZnO diodes with different Er contents in the active region. The observed peaks at 34.46, 36.28, and 31.82° were attributed to ZnO (002), (101), and (100) planes, respectively. No Er-oxide-related peaks[26,27] can be observed. With the increase in Er content, the intensity ratio of (002) to (100) increased and thus the crystalline property varied.

Figure 2 shows the surface morphology of the diodes (a) without Er doping (S0), (b) with 1% Er doping (S1), (c) with 5% Er doping (S2), and (d) with 10% Er doping (S3). For sample S0, the morphology of flakes with different sizes can be observed. With the increase in Er doping content, the number of tiny flakes increases. The result of surface morphology variation is

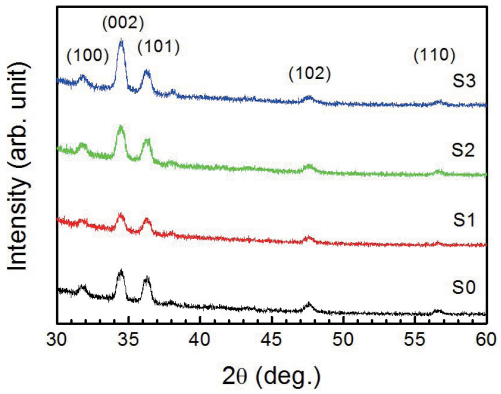

Fig. 1. (Color online) XRD patterns of ZnO diodes without Er doping (S0), with 1% Er doping (S1), with 5% Er doping (S2), and with 10% Er doping (S3).

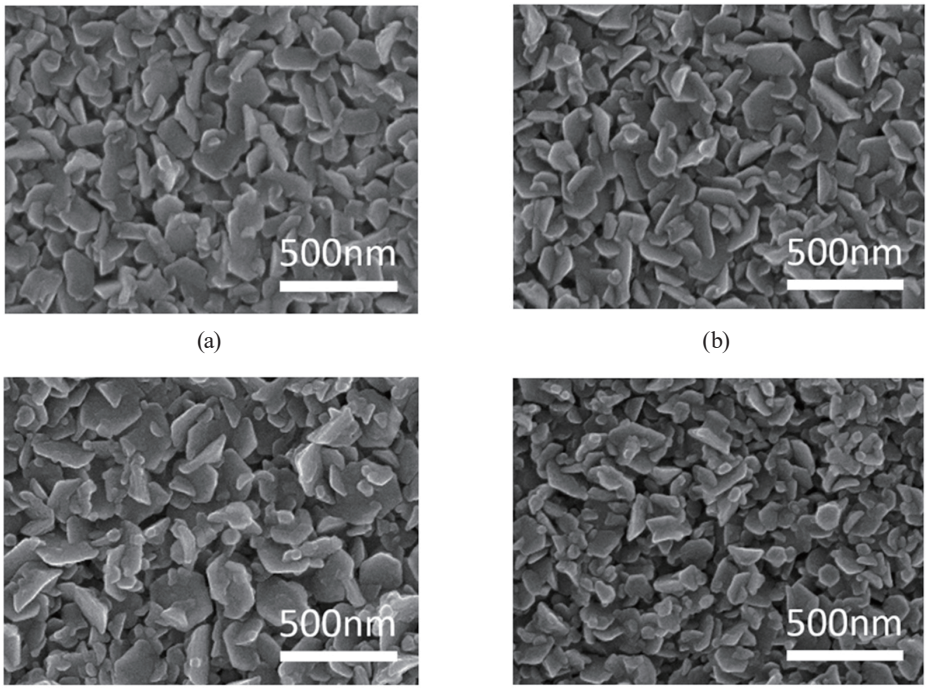

Fig. 2. SEM images of the ZnO diodes (a) without Er doping (S0), (b) with 1% Er doping (S1), (c) with 5% Er doping (S2), and (d) with 10% Er doping (S3).

consistent with the reported grain size shrinkage behavior for the ZnO films with the increase in Er doping content.[18]

Figure 3 shows the 10K PL spectrum of the ZnO diodes. For sample S0, a near-band-edge emission with a peak wavelength of 369.1 nm (3.360 eV) can be observed. This emission is attributed to the recombination of excitons bound to neutral donor (D^oX) and is labeled as bound exciton complexes (denoted as BEC). Another emission band with a wavelength of 373.7

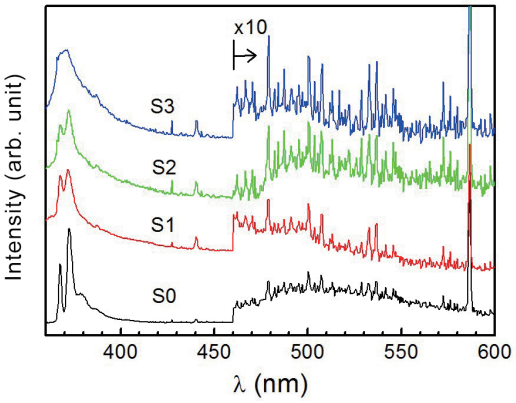

Fig. 3. (Color online) 10K photoluminescence spectrum of ZnO diodes without Er doping (S0), with 1% Er doping (S1), with 5% Er doping (S2), and with 10% Er doping (S3).

nm (3.318 eV) can be observed. This emission, which is around 40 meV below the BEC band, originates from the two electron satellite (denoted as TES) transitions of the D^oX.[28,29] The emission band with a wavelength of 382 nm (3.246 eV), which is 72 meV below TES, is the phonon replica of the TES band (denoted as TES-LO). The emission band with a wavelength of 386.0 nm (3.21 eV), which can be observed in some unintentionally doped ZnO, is attributed to the donor–acceptor pair (denoted as DAP)[29] and/or another TES transition due to a second donor with a different binding energy.[30] Besides, a broad band emission in the wavelength region 460–550 nm can be observed. This band is the combination of deep levels such as ionized oxygen vacancy $[V_O^+]$,[31,32] zinc interstitial state $[Zn_i]$,[33] oxygen antisite state $[O_{Zn}]$,[34] oxygen interstitial level $[O_i]$,[31] and zinc vacancy-related transitions.[34,35]

For samples S1 and S2, with the introduction of Er, the BEC band with a peak wavelength of 373.7 nm as sample S0 can be identified. Besides, an emission band with a peak wavelength of 373.2 nm (3.323 eV) can be observed. For Zn with Er doping, although there is no obvious PL emission band,[36] the incorporation of Er may alter the binding energy of D^oX[25] and cause the energy shift of the TES band. These reveal that the bonding environment varies. For sample S3, with more Er causing binding state variation, a broad near-band-edge emission as the combination of BEC and TES can be observed. Two broad bands around 470–520 nm (denoted as CE) and 510–550nm (denoted as GE) can be observed for the Er-doped samples. The CE band, with the corresponding energy of 2.5 eV, is identified as $[V_O^+]$[31,32] and/or $[Zn_i]$.[33] The GE band, with the corresponding energy around 2.3 eV, is attributed to O_{Zn},[34] O_i,[31] and/or the zinc vacancy-related transitions.[34,35] Thus, the incorporation of Er into the ZnO may alter the structural binding state of the ZnO.

Figure 4 shows the current–voltage (*I–V*) characteristics of these ZnO diodes at room temperature. A rectification character in forward bias and breakdown behavior in reverse bias can be observed.

For a diode with the series resistance *Rs*, the diode *I–V* character is[36]

$$I = I_0(e^{\frac{q(V-I\times Rs)}{n k_B T}} - 1), \tag{1}$$

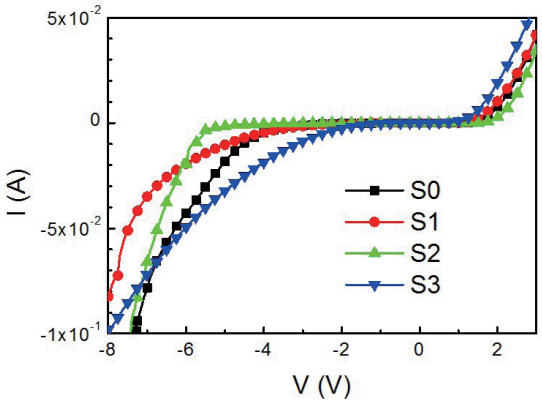

Fig. 4. (Color online) *I–V* characteristics of the ZnO diodes without Er doping (S0), with 1% Er doping (S1), with 5% Er doping (S2), and with 10% Er doping (S3).

where I_0 is the reverse saturation current, q is the electronic charge, k_B is the Boltzmann constant, T is the temperature, and n is the ideality factor. To extract n and Rs from the *I–V* character, one can rearrange the equation to

$$I\frac{dV}{dI} = \frac{n\,k_BT}{q} + I \times Rs. \tag{2}$$

Then, n and Rs can be extracted using the plot of *IdV/dI–I* from the intercept and slope. Figure 5 shows the *IdV/dI–I* plot of the diodes. The extracted n and Rs are listed in Table 1. For the 1% Er-doped ZnO the high Rs value can be observed. The incorporated Er ions may alter the bonding environment as shown in Fig. 3 and thus inhibit the carrier concentration[25] generated from native defects. The reduction-of-defect effect may cause the high ethanol gas sensor response for the 1% Er-doped ZnO.[13] With the increase in Er content higher than 1% in ZnO, the carrier concentration increases as the interstitial of Er to Zn occurred, and Rs decreases to 20.5 Ω (S3). For the ideality factor n, a quantity greater than 2 can be observed for all samples; n is 1 for the recombination of injected carriers in the neutral region and 2 for the carrier recombination by mediated recombination centers in the space charge region.[37,38] The ideality factor n greater than 2 reveals more recombination paths and the diode is far from being ideal.[39] For the heterostructured diode in this work, the high ideality may be caused by the effect of heterojunction[40] and/or the high defect density[18] in the ZnO:Er film.

For the Er-doped diodes operated in reverse bias, a green light emission can be observed with a certain injection current. Figure 6 shows the electroluminescence spectra of samples S1, S2, and S3 with a reverse-biased injection current of 100 mA at room temperature. The inset shows a photo of light emission for sample S2. With spectral measurement, three emission bands in the visible range can be observed. For the diode under reverse bias, as the concentration of p-Si (5×10^{18} cm^{-3}) is higher than the electron concentration of ZnO:Er, the depletion region of the diode is mainly in the ZnO:Er region. The electron–hole pairs, which were created and accelerated in the depletion region by the high electric field, transfer the energy to excite

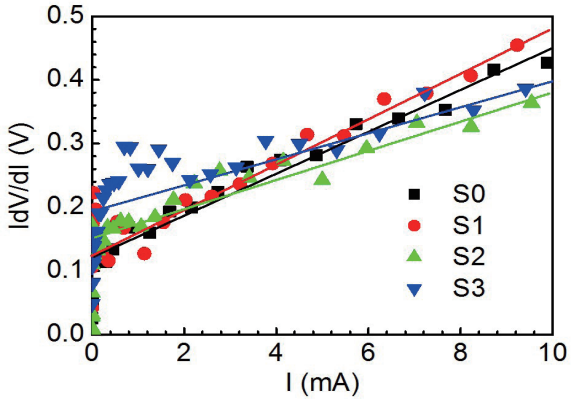

Fig. 5. (Color online) *IdV/dI–I* plot of the ZnO diodes with different Er contents at room temperature.

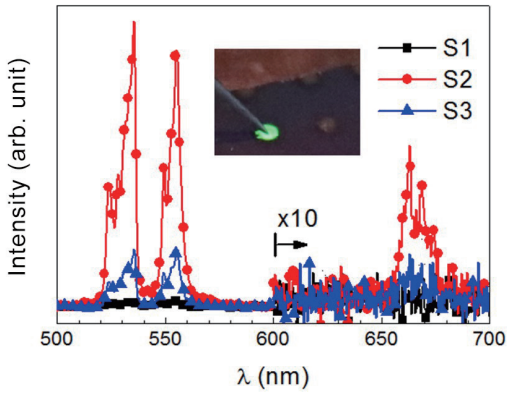

Fig. 6. (Color online) Electroluminescence spectra of the Er doped ZnO diode samples S1, S2, and S3 with 100 mA injection current at room temperature. The inset shows the photo of light emission for sample S2.

Table 1
Structure, ideality factor (*n*), and series resistance (*Rs*) of the ZnO diode with different Er contents. The ratio of Er/Zn in the precursor is shown in the parentheses.

Sample	Structure	*Rs* (Ω)	*n*
S0	p-Si/ZnO/ZnO:In	33.5	4.5
S1	p-Si/ZnO:Er(1%)/ZnO:In	35.6	4.5
S3	p-Si/ZnO:Er(5%)/ZnO:In	22.9	5.8
S4	p-Si/ZnO:Er(10%)/ZnO:In	20.5	7.5

Er ions by impact ionization[41,42] and cause the emissions of the diode. The emission bands are related to the energy state transitions of Er^{3+} of $^2H_{11/2}\rightarrow{}^4I_{15/2}$ (520–540 nm), $^4S_{3/2}\rightarrow{}^4I_{15/2}$ (549–555 nm), and $^4F_{9/2}\rightarrow{}^4I_{15/2}$ (650–670 nm).[43] The fine structure in the emission band is caused by the variation of the host structure.[44] In sample S1, the weak emission intensity may be caused by the low Er content. With the increase in Er content in the diode, the intensity of sample S2 increases and three emission bands can be observed. For sample S3, the intensity decreases and only two emission bands can be observed. The red emission band (650–670 nm) cannot be observed for the diode with high defect density.[45] This reveals the degradation of the film quality of sample S3 and is consistent with the broad near-band-edge emission of PL characterization in Fig. 3.

4. Conclusions

The properties of p-Si/ZnO:Er/ZnO:In diodes with various Er doping contents prepared by spray pyrolysis were studied. The surface morphology and crystalline quality were investigated. With the increase in Er content into ZnO, a broad near-band-edge emission and varied deep-level emissions in PL spectra were characterized. The rectified *I–V* behavior of the diodes was characterized. High diode resistance for 1% Er-doped ZnO in the active region with the inhibition of carrier concentration caused from defects shows extensive potential in

sensor application. With the increase of Er content higher than 1% in the active region, diode resistance decreases, and the incorporation of Er doping also induces certain defect states in the active region. This causes the high ideality factor behavior and thus reduces the diode luminescence efficiency.

Acknowledgments

This research was supported by the Ministry of Science and Technology, Taiwan (MOST 104-2221-E-390-011-MY2, MOST 106-2221-E-390-012), and National Chung Shan Institute of Science and Technology, R.O.C. [NCSIST-103-V304(106)].

References

1 X. Su, Z. Zhang, and M. Zhu: Appl. Phys. Lett. **88** (2006) 061913.
2 R. A. Wahyuono, F. Hermann-Westendorf, A. Dellith, C. Schmidt, J. Dellith, J. Plentz, M. Schulz, M. Presselt , M. Seyring, M. Rettenmeyer, and B. Dietzek: Chem. Phys. **483** (2017) 112.
3 D. A. Lucca, D. W. Hamby, M. J. Klopfstein, and G. Cantwell: Phys. Status Solidi B **229** (2002) 845.
4 H. Yamauchi, M. Iizuka, and K. Kudo: Jpn. J. Appl. Phys. **46** (2007) 2678.
5 D. Choi, M. Y. Choi, W. M. Choi, H. J. Shin, H. K. Park, J. S. Seo, J. Park, S. M. Yoon, S. J. Chae, Y. H. Lee, S. W. Kim, J. Y. Choi, S. Y. Lee, and J. M. Kim: Adv. Mater. **22** (2010) 2187.
6 Z. T. Salim, U. Hashim, M. K. M. Arshad, M. A. Fakhri, and E. T. Salim: Mater. Res. Bull. **86** (2017) 215.
7 J. H. Lim, C. K. Kang, K. K. Kim, I. K. Park, D. K. Hwang, and S. J. Park: Adv. Mater. **18** (2006) 2720.
8 F. H. Nicoll: Appl. Phys. Lett. **9** (1966) 13.
9 K. V. Gurav, M. G. Gang, S. W. Shin, U. M. Patil, P. R. Deshmukh, G. L. Agawane, M. P. Suryawanshi, S. M. Pawar, P. S. Patil, C. D. Lokhandeb, and J. H. Kim: Sens. Actuators, B **190** (2014) 439.
10 X. H. Zhang, J. Chen, Y. Wu, Z. Xie, J. Kang, and L. Zheng: Colloids Surf., A **384** (2011) 580.
11 A. Hastir, N. Kohli, and R.C. Singh: J. Phys. Chem. Solids **105** (2017) 23.
12 B. S. Cao, L. Rino, J. L. Wu, Y. Y. He, Z. Y. Zhang, Z. Q. Feng, and B. Dong: Sens. Actuators, A **268** (2017) 110.
13 Y. Sun, Z. Zhao, P. Li, G. Li, Y. Chen, W. Zhang, and J. Hu: Appl. Surf. Sci. **356** (2015) 73.
14 J. C. Ronfard-Haret, J. Kossanyia, and J. L. Pastol: J. Phys. Chem. Solids **62** (2001) 565.
15 S. Harako, S. Yokoyama, K. Ide, X. Zhao, and S. Komoro: Phys. Status Solidi A **205** (2008) 19.
16 M. Llusca, J. Lopez-Vidrier, S. Lauzurica, M. I. Sanchez-Aniorte, A. Antony, C. Molpeceres, S. Hernandez, B. Garrido, and J. Bertomeu: J. Lumin. **167** (2015) 101.
17 J. C. Ronfard-Haret, J. Kossanyi, and J. L. Pastol: J. Phys. Chem. Solids **62** (2001) 565.
18 S. Iwan, S. Bambang, J. L. Zhao, S. T. Tan, H. M. Fan, L. Sun, S. Zhang, H. H. Ryu, and X. W. Sun: Physica B **407** (2012) 2721.
19 F. Vetrone, J. C. Boyer, J. A. Capobianco, A. Speghini, and M. Bettinelli: Appl. Phys. Lett. **80** (2002) 1752.
20 D. M. Bagnall, Y. F. Chen, M. Y. Shen, Z. Zhu, T. Goto, and T. Yao: J. Cryst. Growth **184** (1998) 605.
21 X. Duan, G. Chen, L. Guo, Y. Zhu, H. Ye, and Y. Wu: Superlattices Microstruct. **88** (2015) 501.
22 T. Shiosaki, S. Ohnishi, and A. Kawabata: J. Appl. Phys. **50** (1979) 3113.
23 L. Spanhel and M. A. Anderson: J. Am. Chem. Soc. **113** (1991) 2826.
24 Y. T. Hsu, W. H. Lan, K. F. Huang, J. C. Lin, and K. J. Chang: Physica B **481** (2016) 63.
25 T. H. Lin, Y. F. Lu, Y. H. Chen, W. H. Lan, M. C. Shih, M. C. Wang, J. C. Lin, K. J. Chang, and W. J. Lin: IEEE Int. Symp. Next-Generation Electronics 2016, Taiwan (2016) 7167.
26 V. Mikhelashvili, G. Eisenstein, and F. Edelmann: Appl. Phys. Lett. **80** (2002) 2156.
27 D. Levchuk, S. Levchuk, H. Maier, H. Bolt, and A. Suzuki: J. Nucl. Mater. **367** (2007) 1033.
28 A. Teke, U. Ozgur, S. Dogan, X. Gu, and H. Morkoc: Phys. Rev. B **70** (2004) 195207.
29 B. K. Meyer, H. Alves, D. M. Hofmann, W. Kriegseis, D. Forster, F. Bertram, J. Christen, A. Hoffmann, M. Strabburg, M. Dworzak, U. Haboeck, and A. V. Rodina: Phys. Status Solidi, B **241** (2004) 231.
30 K. Thonke, T. Gruber, N. Teofilov, R. Schonfelder, A. Waag, and R. Sauer: Physica B **308** (2001) 945.
31 A. C. Rastogi, S. B. Desu, P. Bhattacharya, and R. S. Katiyar: J. Electroceramics **13** (2004) 345.
32 J. C. Fan, K. M. Sreekanth, Z. Xie, S. L. Chang, and K. V. Rao: Prog. Mater. Sci. **58** (2013) 847.

33 J. C. Sun, H. W. Liang, and J. Z. Zhao: Chem. Phy. Lett. **460** (2008) 548.
34 A. S. Gadallah and M. M. E. Nahass: Adv. Condens. Matter Phys. **1** (2013) 234546.
35 S. Golshahi, S. M. Rozati, R. Martins, and E. Fortunato: Thin Solid Films **518** (2009) 1149.
36 E. Fred Schubert: Light-Emitting Diodes (Cambridge University Press, New York, 2006) 2nd ed., p. 64.
37 J. M. Shah, Y. L. Li, T. Gessmann, and E. F. Schubert: J. Appl. Phys. **94** (2003) 2627.
38 C. T. Sah, R. N. Nyoce, and W. Shockley: Proc. IRE (1957) 1228.
39 N. Zebbar, Y. Kheireddine, K. Mokeddem, A. Hafdallah, M. Kechouane, and M. S. Aida: Mater. Sci. Semicond. Process. **14** (2011) 229.
40 D. Zhu, J. Xu, A. N. Noemaun, J. K. Kim, E. F. Schubert, M. H. Crawford, and D. D. Koleske: Appl. Phys. Lett. **94** (2009) 081113.
41 J. M. Langer, A. Lemanska-Bajorek, and A. Suchocki: Appl. Phys. Lett. **39** (1981) 386.
42 G. Franzo, S. Coffa, F. Priolo, and C. Spinella: J. Appl. Phys. **81** (1997) 2784.
43 S. Prucnal, L. Rebohle, and W. Skorupa: J. Non-Cryst. Solids **357** (2011) 915.
44 A. Polman: Physica B **300** (2001) 78.
45 S. Harako, S. Yokoyama, K. Ide, X. Zhao, and S. Komoro: Phys. Status Solildi A **205** (2008) 19.